Evaluation of the temporal effect to the peak tailing in flow injection analysis

Su-Cheng Pai*

Division of Marine Chemistry, Institute of Oceanography, National Taiwan University, P.O. Box 23-13, Taipei, Taiwan

Abstract

The deformation of a flow injection analysis peak from a Gaussian shape has two components: spatial and temporal. The former is mainly attributed to the Poisseulie effect in the tubular flow, whereas the latter is related to the observing position (of a fixed detector) at which signal is measured. The combination of the two makes a skewed peak track on the recorder chart. Therefore, an observed peak may imply a substantial fraction of a ''false'' tail due to the effect of non-simultaneous detection. An expanding-Gaussian model is proposed to simulate the purely temporal effect, and the asymmetric factors were compared with that of the experimental peak shapes. In most cases the peak deformation occurring in flow injection analysis should be regarded as ''temporal''. The contribution of the spatial effects (Poisseulie profile and others) might not be as significant as it was thought previously. © 2002 Elsevier Science B.V. All rights reserved.

Keywords: Peak tailing; Flow injection analysis; Temporal effect

1. Introduction

Many chemical instruments give output signals as peaks. In chromatography the peak is generally symmetrical or Gaussian-like, but for flow injection analysis (FIA) it is frequently skewed with a tail. The tailing phenomenon, important for optimizing instrumental conditions, has drawn intensive attention since the technique was introduced in 1975 [1]. A question is raised: why is the FIA peak asymmetrical? One may seek assistance from existing chromatographic theories as both techniques share very much the same physical principles [2]. Several chromatographic models are helpful in this respect including the progressively calculated plate [3] or tank-in-series model [4], the stochastic statistical model [5], and the solutions of the partial differential equations for mass transfer kinetics along a column [6–8]. However, after a numerical comparison Golshan-Shirazi and Guiochon [9] concluded that all chromatographic models can be approximated by a Gaussian profile even when the column efficiency is low. Although each model does give an asymmetrical peak shape at the initial stage, the skewness is considered ''insignificant'', far from enough to justify the observations commonly seen in FIA work.

Further explanations become complex. The concept of ''non-linear isotherms'' have been used in adsorption chromatography to derive non-symmetrical peaks [10], but it surely cannot be valid for FIA due to the lack of a stationary phase. Instead, the physical models derived from Fick's Law [11–15], which is based on the physical dispersion–diffusion

*Tel.: +886-2-2362-7358; fax: +886-2-2363-2912.
E-mail address: scpai@ccms.ntu.edu.tw (S.-C. Pai).

behaviors of a tubular flow, have been more favored. Together with the friction effect against the tube wall, the resultant "Poisseulie" or the "parabolic velocity" profile has been generally adopted as the major source for the peak tailing in flow injection analysis, and the "bow-shape" diagram appears frequently in papers and textbooks [1,16].

1.1. The observer's position

One important factor, the observer's effect or the temporal effect, might have been overlooked by FIA analysts. When a shape-changing object passes through a fixed narrow-slit scanning camera, the observer will receive a distorted picture. It relates only to the observer's standing point and the movement of that object, and not to the real appearance of the object at a time. The deformation due to the non-simultaneous detection is spatially "false". An "observed peak shape" implies the "real peak shape" plus "temporal deformation". The concept is not novel in the chromatographic field. Back in the 1950s, a continuous plate theory given by Glueckhauf [17] has already demonstrated that the peak shape can be distorted to have a tail even when the mass distribution in a column is Gaussian. A worksheet practice of the Glueckauf's model is included in a recent textbook by de Levie [18].

Misinterpretation might start from here: some FIA analysts tend to use experimentally observed peak shape to represent the mass-distribution pattern in the tubing, as they deemed the difference is negligible. Indeed, the mass distribution curve, based on a length coordinate, can be converted to a time scale. For example, the mean residence time or peak appearance time t_p can be calculated from $t_p = \pi r^2 L/F$ (where r is the tube radius, L the length of the tubing, F the flow-rate) or $t_p = L/u$ (u the flow speed). This "converted" time coordinate, although having identical scaling to that on the "observer's" time coordinate, is still spatial in nature. Without making a distinction between the two may lead to further confusion when dealing with the peak shape problems.

2. Theoretical
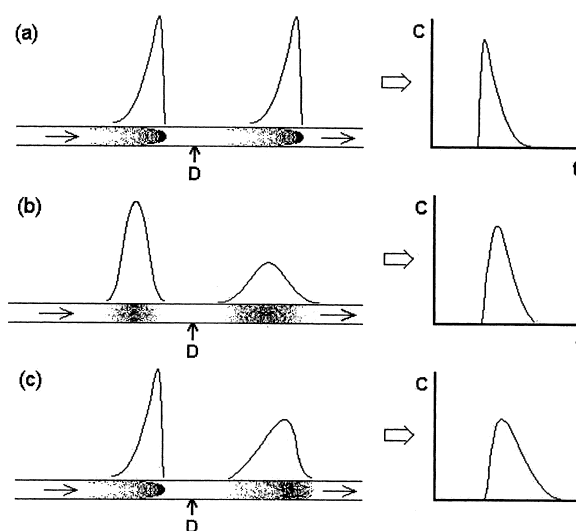
A diagram (Fig. 1) is presented to distinguish the

Fig. 1. Diagrams illustrating the possible relationships between the mass profile (left) and recorded peak shape (right). (a) Assuming that the mass distribution in the tubular channel is asymmetrical due to the Poisseulie effect, and that the pattern is unchanged during its passage through the detector at position D, the recorder will give peak shape exactly like the mass distribution peak. The deformation of peak is purely spatial. (b) Assuming the mass distribution is symmetrical throughout but the sample zone is expanding while moving, the detector will record a steeper peak front and a prolonged peak tail. The deformation of peak is purely temporal. (c) In real situation the skewed peak image might attribute to the combination of both.

"spatial profile" and "temporal deformation". They are separated on a hypothetical basis. In the former case (Fig. 1a), the injected sample section moves faster at the center axis than near the tube wall, leading to an asymmetric distribution pattern. If the pattern remains unchanged during its passage through a detector, a skewed shape is recorded. The image reflects a purely spatial pattern. In the latter case (Fig. 1b), if the injected sample section has already become a Gaussian-like pattern soon after leaving the injector, and it is still broadening with time as it travels, the sensor encounters first a steeper front and then records a prolonged tail when the main peak passes over. The deformation of the observed peak is purely temporal.

In a real situation, the skewness of a peak should refer to the combination of the two processes (see Fig. 1c). However, since one can always derive the asymmetrical parabolic laminar flow by equations, only the spatial effect has been emphasized by FIA

modelists. The temporal effect, sounds insignificant and difficult to verify experimentally, has been usually ignored.

2.1. Mathematical approach

For laboratory applicants, the mathematical approaches are of value if they can be simple enough to be practiced on a computer spreadsheet (e.g., Excel). The most successful one would be the exponentially modified Gaussian function (EMG) [19–22]. It is based on the fact that all complicated models converge to a Gaussian function, and the degree of deformation decays exponentially with time. Thus, through a convolution process, an EMG curve is generated (in Gaussian form plus decay function). The EMG function can indeed produce significant asymmetric peak shape even at high theoretical plate numbers. Even though the physical meaning has been questioned by some scientists [9], it has been widely adopted as a reasonable approach in the chromatography field [23].

2.2. Conceptual approach

A more simple approach is described in this work namely, the expanding-Gaussian function. It follows the posture of the EMG function that the mass profile in a tubular channel is eventually Gaussian. Instead of converging an exponential function, the Gaussian curve is "transformed" from a spatial axis to a temporal axis. The skewness of the observed peak is generated by the Gaussian curve itself, as it expands while it moves. Therefore, the present model is more a "conceptual" one than a mathematical fitting.

Only two basic equations are involved: a standard Gaussian equation, and one describing the expanding of its standard deviation along the x-axis. In FIA, x can be the length L of the tubular channel or time t. According to previous theories, the "zone-broadening" of a Gaussian profile can be defined as the expanding of the standard deviation σ_L of the peak, which is proportional to the square root of the travel distance L at a constant flow speed (or $\sigma_L^2 \propto L$):

$$\sigma_L = \mu_L \sqrt{L} \tag{1}$$

where μ_L is defined here as an "expanding coefficient" (on L coordinate) of the flow system. (Note

that this coefficient, in $cm^{1/2}$ unit, is equivalent to the square root of the theoretical plate height H_L in chromatography. It also equals $\sqrt{2D/u}$ in Fick's law where D is the diffusion coefficient and u the flow speed [23]. The purpose of using of μ_L or later μ_t in this paper is to emphasize the "expanding" nature of the injected sample zone, just for the convenience of FIA readers.)

2.3. Spatial distribution profile

Combining Eq. (1) and a standard Gaussian equation and letting the total peak area as A_L, a symmetric concentration distribution pattern $C(L)$ at a given time is generated and it can be plotted on the L coordinate:

$$C(L) = \frac{A_L}{\mu_L\sqrt{2\pi L_p}} e^{-\left(\frac{L-L_p}{\mu_L\sqrt{2L_p}}\right)^2} \tag{2}$$

where L_p is the position of peak summit (usually refers to the position of the detector on the L coordinate). The curve generated by Eq. (2), noted as the mass distribution curve, cannot be observed temporally by a single fixed detector. It could only be seen if there were "many" detectors set along the channel to detect simultaneously.

It is very easy for one to think that Eq. (2) can be converted into time scale, as t_p is proportional to $L_p(t_p = L_p/u)$, and $\sigma_t^2 \propto t_p$; A_L and μ_L can be transformed into temporal terms A_t and μ_t correspondingly. Thus, it can be "mistakenly" expressed as:

$$C(t) = \frac{A_t}{\mu_t\sqrt{2\pi t_p}} e^{-\left(\frac{t-t_p}{\mu_t\sqrt{2t_p}}\right)^2} \tag{3}$$

This Gaussian-type curve, although on a time scale, does not reveal the recorder output, as what the detector receives should be on a "sequential" time axis. Therefore the peak generated by Eq. (3) does not exist and should not be plotted.

2.4. Temporal convolution

To project the non-existing image of Eq. (3) from a "simultaneous" time coordinate to a "real" time coordinate is named the "temporal convolution". Since the observation is made at a single point, one should consider the standard deviation of a peak (σ_t) is variable at all time ($\sigma_t \propto \sqrt{t}$ instead of $\sigma_t \propto \sqrt{t_p}$). It

means that the observed curve is composed of many mass–curve segments at various time t. Thus, by replacing t_p as t in the square root terms, a "spatial-temporal projection-transformation equation", or simply the "temporally convoluted Gaussian" (TCG) is given:

$$C(t) = \frac{A_t}{\mu_t\sqrt{2\pi t}}\, e^{-\left(\frac{t-t_p}{\mu_t\sqrt{2t}}\right)^2} \qquad (4)$$

The peak generated by this TCG equation is not symmetrical, but it reveals the output on a recorder chart. The temporal deformation fraction of Eq.(4) from a Gaussian profile can be defined as the difference between Eqs. (3) and (4):

$$TD(t) = \frac{A_t}{\mu_t\sqrt{2\pi t}}\, e^{-\left(\frac{t-t_p}{\mu_t\sqrt{2t}}\right)^2} - \frac{A_t}{\mu_t\sqrt{2\pi t_p}}\, e^{-\left(\frac{t-t_p}{\mu_t\sqrt{2t_p}}\right)^2}$$

$$(5)$$

where $TD(t)$ is the temporal deformation function. It has three "crossing knots" on the t axis, one near the peak summit, and the rest two at each side of the peak (Fig. 2). The skewness of a peak relates to both
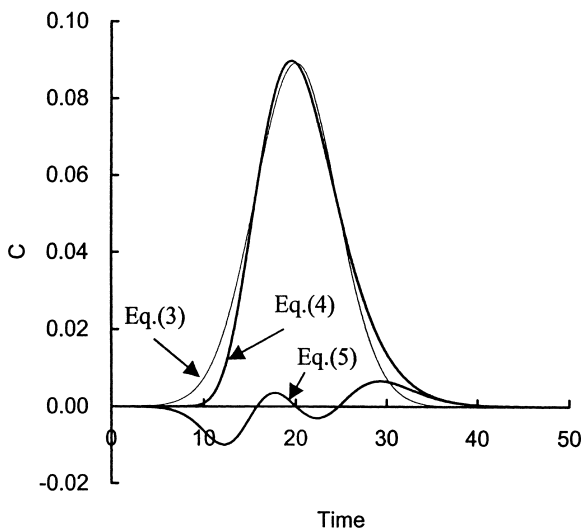

Fig. 2. The temporal deformation function, $TD(t)$ (Eq. (5)) is the difference between a standard Gaussian curve (Eq. (3)) and the TCG curve (Eq. (4)). Assuming $\mu_t = 1$, $A_t = 1$, and $t_p = 20$, the curve crosses t-axis at $t = 15.8$, 20.0 and 24.7. The temporal peak ($t_p^* = 19.5$, $h = 0.0898$) appears slightly earlier than that expected ($t_p = 20$, $h = 0.0892$), with a slightly higher peak height.

t_p and μ_t, to be significant when t_p is small or μ_t is large, and vice versa.

2.5. Temporal shift of peak summit

It is interesting to find that the position of the temporally convoluted peak (note as t_p^*) appears slightly earlier than t_p; thus it has an identical peak height to that of the spatial peak at t_p but with a "very" slightly higher peak height at t_p^*. The small temporal shift ($t_p - t_p^*$) is related to μ_t but independent to A_t or t_p. The scale is ca. 0.5 s when $\mu_t = 1.0$ s$^{1/2}$ at a constant flow speed, 0.4 s when $\mu_t = 0.9$ s$^{1/2}$, and 0.3 s when $\mu_t = 0.8$ s$^{1/2}$. The expanding coefficient μ_t may vary from system to system. A quick estimation can be made experimentally by measuring the "observed" peak area A_t, height h, and position t_p^*:

$$\mu_t \approx A_t/h/\sqrt{2\pi t_p^*} \qquad (6)$$

In most FIA cases μ_t should be around 1 s$^{1/2}$.

2.6. Comparison to previous models

The TCG equation generates promising asymmetric peaks but with no surprise. This conceptual approach, without needing the knowledge of the theoretical plate number, physical diffusion–dispersion or differential equations, leads to a resultant form almost the same as the famous Taylor–Aris series experiment [11,24], also as that derived by Lapidus and Amundson [6] for tubular chromatography. The skewed pattern generated is comparable to that by other sophisticated models as illustrated in the review paper by Golshan-Shirazi and Guiochon [9]. The TCG function is simpler than the EMG function, yet offers similar and reasonable skewed peak shapes.

The question becomes: is the zone broadening symmetrical at the very beginning and throughout, and the observed tail a "false" one due to the temporal effect? Or, is the zone broadening not symmetrical initially, turning to be Gaussian but still viewed as having a temporal tail? Or, does the asymmetric zone broadening accompany with the temporal effect at all time? If both spatial and temporal components co-exist as stated in Fig. 1c,

analysts would like to know: which is dominating in FIA?

3. Experimental

To further verify the temporal effect by experiment, a simplified flow injection system was assembled as shown in Fig. 3. It comprised a peristaltic pump running a distilled water carrier at a constant rate of 4.25 ml/min; a Rheodyne four-way injector having an injection volume of 0.357 ml; a Hitachi U-2000 double-beam spectrophotometer installed with a Hellma narrow-bore flow cuvette (light path 1.0 cm, capacity 31 µl); a delay coil that connected between the injector and the detector. A series of delay coil of variable lengths (20–360 cm) was made using PTFE tube of 0.8 mm I.D. wound onto a supporting rod. The coiled tubing facilitates mixing in the flow channel [1].

A blue dye solution was used as the testing sample; the undiluted absorbance reading was 0.805 (at $\lambda_{max} = 629$ nm). Upon the injection of the dye solution (vol.=0.357 ml), the recorder was pressed "on" to draw the peak track. Each resultant peak was specified by measuring its peak appearance time (t_p^*), peak height (h), and all those parameters useful to characterize the peak asymmetry [25] (see Fig. 4), i.e., peak widths ($W_{0.1}$ and $W_{0.5}$) at $0.1h$ and $0.5h$ levels, respectively, components (a, b, c, d) and their corresponding positions (t_a, t_b, t_c, t_d).

4. Results and discussion

4.1. Experimental peaks

The recorded peak shapes (with delay coil lengths $L = 0$, 20, 40, 60, 80, 100, 120, 140, 160, 200, 260, 300, 360 cm, respectively) obtained by the proposed flow injection system are shown in Fig. 5. The peak information is listed in Table 1. The peak area was estimated to be 4.06 by taking the multiplied value of the initial bandwidth and absorbance of the injected sample. The expanding coefficient μ_t was estimated from Eq. (6), to be 1.01 ± 0.037 s$^{1/2}$ for this system. The "observed" peak positions were
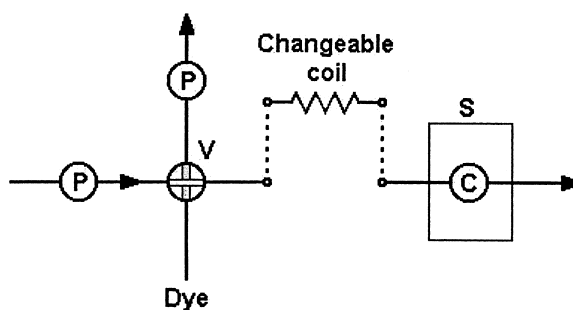

Fig. 3. Layout of the flow injection system used in this study. The delay coil is changeable from 0 to 360 cm long (made of PTFE tube 0.8 mm I.D.). P, peristaltic pump; V, injection valve; S, spectrophotometer; C, 1 cm flow cuvette (capacity 31 µl).

regarded as t_p^*, whereas the "spatial" position t_p were retrieved by adding to t_p^* a temporal shift of 0.5 s.

4.2. TCG simulations

By taking the experimental A_t, μ_t, and corresponding t_p values (Table 1), and putting into the temporally convoluted Gaussian (TCG) equation, a series of peaks was generated (Fig. 6). The asymmetry components (a and b) were obtained by analyzing the TCG peak at $0.1h$ level (at $t_p^* - a$ and $t_p^* + b$). All simulated peak data are listed in Table 2.
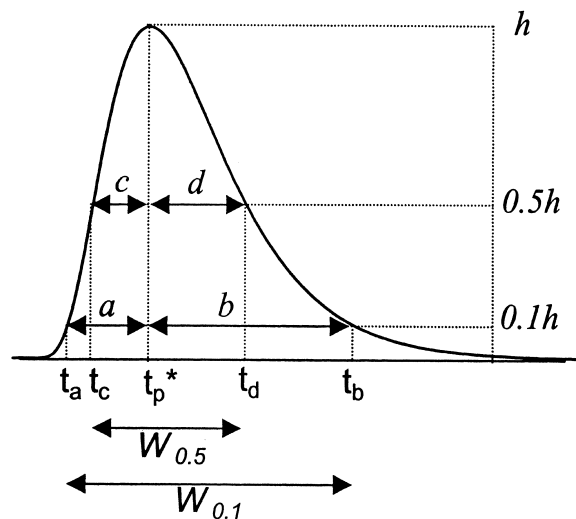

Fig. 4. Parameters of an experimental asymmetrical peak. Asymmetry factor (A_f) is defined by $A_f = b/a$.
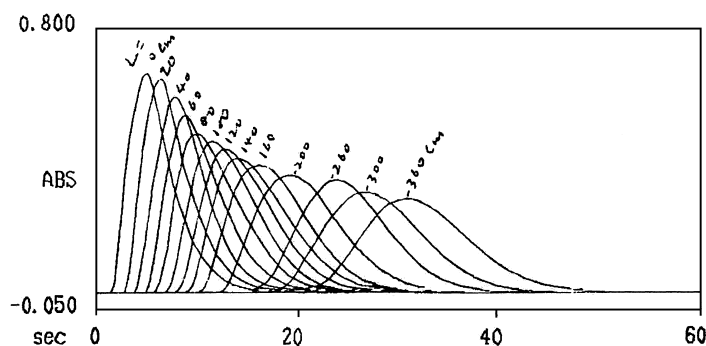
Fig. 5. The peak tracks recorded by a Hitachi U-2000 spectrophotometer for a dye sample injected into the flow injection system with variable delay coil lengths. The injection volume was 0.357 ml. The lengths of delay coils were manually marked on the chart.

Table 1
Parameters taken from experimental peaks shown in Fig. 5

| Coil length L_c (cm)	Peak height h (Abs)	Peak position observed (s)					Peak width		Skewness			μ_t estimated by Eq. (6)	Spatial t_p
		t_a	t_c	t_{p*}	t_d	t_b	$W_{0.5}$	$W_{0.1}$	a	b	$A_f = b/a$		
0	0.667	2.0	3.4	5.7	8.3	11.4	4.9	9.4	3.7	5.7	1.541	1.02	6.2
20	0.646	3.4	4.8	7.1	10.0	13.0	5.2	9.6	3.7	5.9	1.595	0.94	7.6
40	0.593	4.4	5.8	8.4	11.8	15.4	6.0	11.0	4.0	7.0	1.750	0.94	8.9
60	0.524	5.5	7.2	9.7	13.7	17.0	6.5	11.5	4.2	7.3	1.738	0.99	10.2
80	0.475	6.5	8.0	10.8	15.4	18.8	7.4	12.3	4.3	8.0	1.860	1.04	11.3
100	0.459	7.6	9.5	12.2	17.0	20.7	7.5	13.1	4.6	8.5	1.848	1.01	12.7
120	0.434	8.7	10.6	13.5	18.6	22.5	8.0	13.8	4.8	9.0	1.875	1.02	14.0
140	0.404	9.9	11.6	14.9	20.1	24.2	8.5	14.3	5.0	9.3	1.860	1.04	15.4
160	0.382	11.0	13.1	16.5	22.0	26.1	8.9	15.1	5.5	9.6	1.745	1.04	17.0
200	0.353	13.5	15.6	19.5	25.3	29.6	9.7	16.1	6.0	10.1	1.683	1.04	20.0
260	0.341	17.3	20.0	24.4	30.4	35.4	10.4	18.1	7.1	11.0	1.549	0.96	24.9
300	0.301	19.3	22.0	27.2	33.6	39.1	11.6	19.8	7.9	11.9	1.506	1.03	27.7
360	0.281	23.0	26.0	31.5	38.3	43.9	12.3	20.9	8.5	12.4	1.459	1.03	32.0
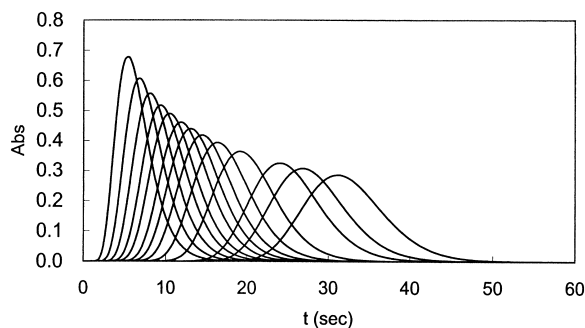
Fig. 6. The observer's FIA peaks generated by Eq. (4) assuming $A_t = 4.06$, $\mu_t = 1.01$, and variable spatial peak positions ($t_p = 6.2$–32 s, respectively, taken from Table 1). All curves were spatially Gaussian before convoluted to the time coordinate. The deformation of the peak shape attributes completely to the temporal effect.

The resemblance of the simulated peak shapes (Fig. 6) to the experimental peaks (Fig. 5) is generally good. They all show characteristics (see Fig. 7) matching the basic FIA rules as stated in textbook by Růžička and Hansen [1]: (1) the shape is skewed when the mean residence time t_p^* is short; and turns gradually to a more symmetrical-look when t_p^* is large; (2) the peak area remains the same at all times; (3) The peak height h decreases with increase of the mean residence time t_p^*; (4) the peak widths ($W_{0.5}$, $W_{0.1}$ or a, b) increase with the square root of t_p^*. However, discrepancies are obvious when t_p^* is very short, say, in the first 10 s in this work, and they should be regarded as the "sample size" effect.

Table 2
Simulated peaks generated by Eq. (4) using $A_t = 4.06$, $\mu_t = 1.01$, and corresponding t_p values in Table 1 (also see Fig. 6)

Spatial t_p (s)	Peak height h (Abs)	Peak position calculated (s)					Peak width		Skewness		
		t_a	t_c	t_{p*}	t_d	t_b	$W_{0.5}$	$W_{0.1}$	a	b	$A_f = b/a$
6.2	0.657	2.48	3.58	5.70	9.17	13.38	5.59	10.90	3.22	7.68	2.385
7.6	0.592	3.32	4.64	7.10	10.92	15.38	6.28	12.06	3.78	8.28	2.190
8.9	0.545	4.15	5.67	8.40	12.50	17.18	6.83	13.03	4.25	8.78	2.066
10.2	0.508	5.00	6.71	9.70	14.06	18.95	7.35	13.95	4.70	9.25	1.968
11.3	0.483	5.75	7.60	10.80	15.38	20.42	7.78	14.67	5.05	9.62	1.905
12.7	0.455	6.72	8.76	12.20	17.02	22.25	8.26	15.53	5.48	10.05	1.834
14.0	0.433	7.66	9.85	13.50	18.54	23.94	8.69	16.28	5.84	10.44	1.788
15.4	0.412	8.65	11.02	14.90	20.15	25.75	9.13	17.10	6.25	10.85	1.736
17.0	0.392	9.83	12.38	16.50	22.00	27.78	9.62	17.95	6.67	11.28	1.691
20.0	0.361	12.07	14.96	19.50	25.42	31.53	10.46	19.46	7.43	12.03	1.619
24.9	0.323	15.86	19.24	24.40	30.95	37.56	11.71	21.70	8.54	13.16	1.541
27.7	0.306	18.07	21.71	27.20	34.08	40.95	12.37	22.88	9.13	13.75	1.506
32.0	0.285	21.53	25.54	31.50	38.85	46.10	13.31	24.57	9.97	14.60	1.464

Note that the appearance of the peak (t_p^*) is 0.5 s earlier than the spatial t_p.

4.3. The sample size effect

It is common to use larger injection size in FIA (compared to chromatography) to avoid losing sensitivity. Therefore the injection volume cannot be treated like a small plug. Instead, the sample section should be regarded to have a histogram-shape at the beginning; which gradually becomes a plateau, then a peak shape when t_p^* becomes large. Taking the present case for instance, the injection volume was 0.357 ml, at a flow-rate of 4.25 ml/min it equals an initial zone width (W_i) of ca. 5 s on the time scale.

Accordingly, the TCG function is derelict within 10 s due to the large sample size. For example, the initial absorbance of the dye was 0.805; but the TCG simulation gives infinite h when t_p is zero (Fig. 7b). Also, experimentally the initial width components a and b were both 2.5 s, leading to an initial $A_f = 1$, while the TCG gives infinite A_f at $t_p^* = 0$ because the initial band width is assumed zero (Fig. 7c). The difference on the peak shapes in the first 10s (or $L_c < 20$ cm) is also noticeable. Experimental peaks are fatter at the middle, whereas simulated peaks have much slender looks even though the bottom ($W_{0.1}$) is wider.

4.4. Comparison on asymmetry factor

Further comparison was done on peaks with t_p^*

larger than 10 s ($t_p^*/w_i > 2$) to skip the sample size effect. Although the digitizing of the experimental peak widths might not be very precise, it does give clear trends as can be seen in Fig. 7. Both a and b components gradually merge with the theoretical lines when t_p^* is larger than 15 s. Within the range of 10–20 s the asymmetry factor ($A_f = b/a$) for the experiment peak is slight larger than of the TCG simulation. Therefore, the temporal effect may not be, although dominant, the only one that controls the peak tailing.

The contributions by the temporal effect have been estimated by taking ($A_f - 1$) as a parameter (Fig. 7d). For peaks with t_p^* between 15 and 20 s ($t_p^*/W_i = 3$–4), the temporal effect conveys a contribution of >90% for the experimental deformation, leaving less than 10% for other effects. When t_p^* is above 25 s ($t_p^*/W_i > 5$), the temporal contribution raises in proportion to nearly 100%, but reduces in scale.

4.5. A general aspect for FIA peaks

Based on the above verifications, a general aspect for the FIA peak shape development stands out and it can be stated in four stages:

Stage 1: At the initial stage or when t_p^* is close to the initial zone width W_i ($t_p^*/W_i < 2$ in the present work), the sample size effect is the major concern,
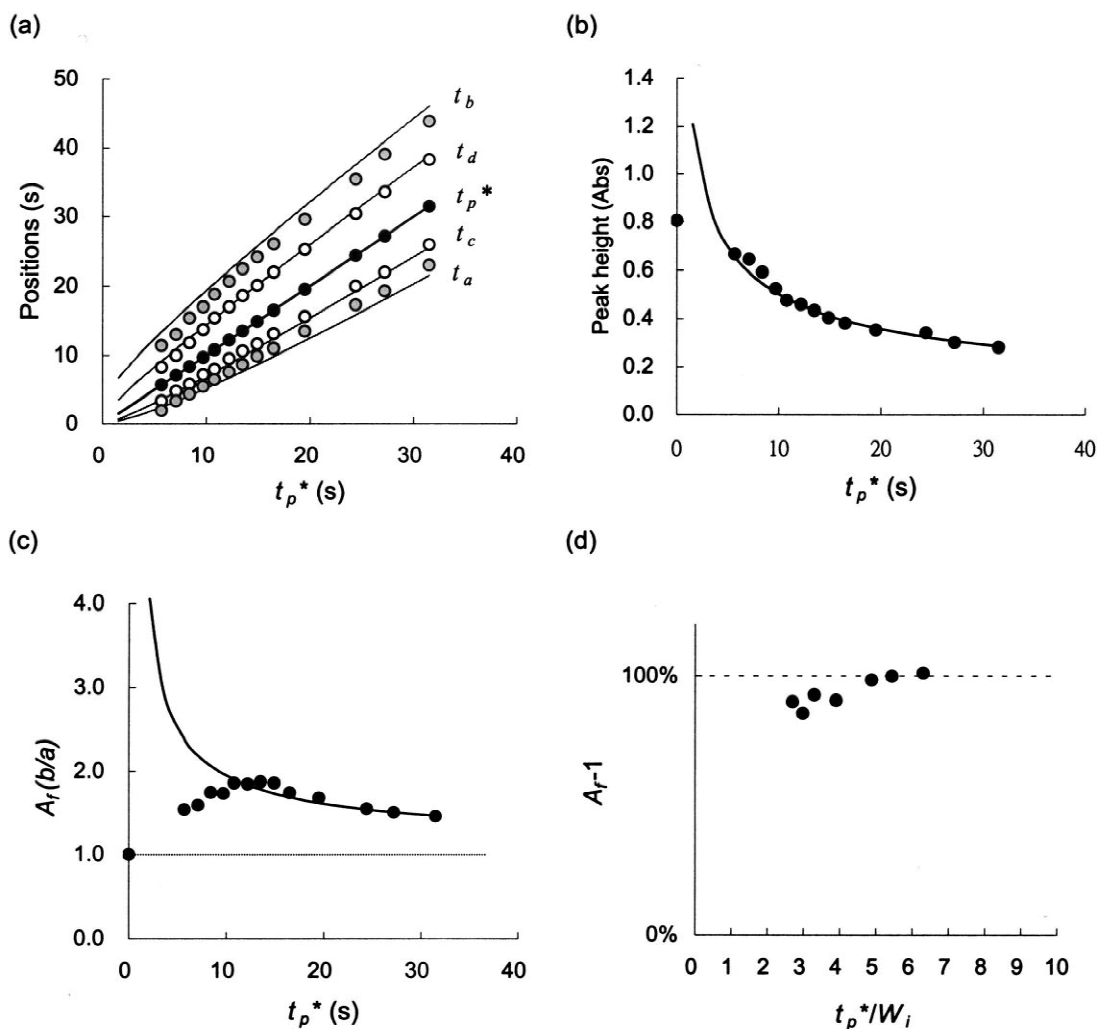
Fig. 7. Comparison of parameters estimated from the observed peaks (circles) and from that generated by TCG equation (lines). (a) Position of t_a, t_b, t_c, t_d versus t_p^*; (b) peak height versus t_p^*; (c) asymmetric factor, $A_f = b/a$, versus t_p^*; (d) temporal contribution ($A_f - 1$) versus t_p^*/W_i.

which gives a plateau-shape pattern and masks all other effects.

Stage 2: When t_p^* is larger (e.g., $t_p^*/W_i > 2$ in this work), the initial sample zone becomes a peak, appearing with an asymmetrical tail. Both spatial (e.g., the sample size effect and the Poisseulie effect) and temporal components may co-exist and co-responsible for the peak skewness.

Stage 3: When t_p^* is even larger ($t_p^*/W_i > 5$ in this work), the spatial effects fade gradually leading to a Gaussian-like distribution in the tubular channel, but

it is still viewed to have a tail on the recorder chart. The temporal effect becomes the dominating reason for the peak deformation.

Stage 4: When t_p^* is very large (say, $t_p^*/W_i > 50$), the asymmetry factor A_f converges to 1 and the peak appearance becomes a Gaussian curve. Neither the spatial nor temporal effect is significant, the observed peak shape reveals almost the same pattern as the mass profile.

In FIA application, it is quite common to have an injection size of 0.1–0.5 ml and a residence time of

30 s–2 min for a sample peak. If the manifold is operated at a flow-rate of 5 ml/min, the t_p^*/W_i ratios lay in a range between 5 and 50 (i.e., stage 3). With this in mind one may consider that most of the peak skewness observed for FIA should be regarded as temporal. For chromatography the t_p^*/W_i is usually very large (>100), the temporal peak tailing can only be observed for those leading peaks at near the void position.

5. Conclusion

There are no contradictions between the proposed TCG equation and existing theories for chromatography and for FIA, as all lead to the same conclusion: the peak is skewed when time is short and gradually turns to a Gaussian-like curve when the time is prolonged. The difference would be that the present work "emphasizes" the temporal effect, which transforms the mass distribution profile from a spatial axis to a sequential time axis and gives a twisted peak shape on the recorder. It provides clues for those who are not familiar enough with physical or mathematical skills to understand when and why is the peak not symmetrical.

The temporal effect exists universally in either FIA or chromatography. However, it seems that many scientists of both fields have neglected this effect completely, leading to contradictions when they need to explain "unexpected" peak tailings: chromatographers tend to explain in a kinetic way, whereas FIA users tend to elucidate on the Poisseulie effect. This could have been arisen from the recognition of the theoretical plate numbers. For example, FIA may have apparent smaller plate numbers due to the lacking of stationary phase and faster flow-rate. However, it should be borne in mind that the scaling is artificially defined, therefore direct comparison on plate numbers might not be appropriate.

The use of "time" as a parameter to evaluate the zone broadening is deemed more practical. Any disparity from the TCG curve could account for the contribution other than the temporal effect.

References

[1] J. Růžička, E.H. Hansen, in: Flow Injection Analysis, 2nd ed, Wiley, New York, Chichester, Brisbane, Toronto, Singapore, 1988.
[2] J. Růžička, G.D. Christian, Analyst 115 (1990) 475.
[3] L.C. Craig, J. Biol. Chem. 155 (1944) 519.
[4] A.J.P. Martin, R.L.M. Synge, Biochem. J. 35 (1941) 1358.
[5] J.C. Giddings, H. Eyring, J. Phys. Chem. 59 (1955) 416.
[6] L. Lapidus, N.L. Amundson, J. Phys. Chem. 56 (1952) 984.
[7] G. Carta, Chem. Eng. Sci. 43 (1988) 2877.
[8] J.B. Rosen, J. Chem. Phys. 20 (1952) 387.
[9] S. Golshan-Shirazi, G. Guiochon, in: F. Dondi, G. Guiochon (Eds.), Theoretical Advancement in Chromatography and Related Separation Technqiues, Kluwer, Dordrecht, Boston, London, 1991.
[10] K. Robards, P.R. Haddad, P.E. Jackson, in: Principles and Practice of Modern Chromatographic Methods, Academic Press, London, Boston, San Diego, New York, Toronto, Sydney, Tokyo, 1994.
[11] G. Taylor, Proc. R. Soc. London, Ser. A 219 (1953) 186.
[12] R. Tijssen, Anal. Chim. Acta 114 (1980) 71.
[13] J.M. Reijn, W.E. van der Linden, H. Poppe, Anal. Chim. Acta 114 (1980) 105.
[14] J.T. Vanderslice, K.K. Stewart, A.G. Rosenfeld, D.J. Higgs, Talanta 28 (1981) 11.
[15] S.H. Isaac, H. Soeber, L.H. Cristensen, J. Villadsen, Chem. Eng. Sci. 47 (1992) 1591.
[16] D.A. Skoog, F.J. Holler, T.A. Nieman, in: Principles of Instrumental Analysis, 5th ed, Saunders College Pub./Harcourt Brace College Publishers, Philadelphia/Orlando, 1998.
[17] E. Glueckauf, Trans. Faraday Soc. 51 (1955) 34.
[18] R. de Levie, in: Principles of Quantitative Chemical Analysis, McGraw-Hill, International Editions, New York, 1997.
[19] J.P. Foley, J.G. Dorsey, J. Chromatogr. Sci. 22 (1984) 40.
[20] D. Hanggi, P. Carr, Anal. Chem. 57 (1985) 2394.
[21] J.P. Foley, J.G. Dorsey, Anal. Chem. 55 (1983) 730.
[22] J.P. Foley, Anal. Chem. 59 (1987) 1984.
[23] D.C. Harris, in: Quantitative Chemical Analysis, 4th ed, W.H. Freeman, San Francisco, CA, 1995.
[24] R. Aris, Chem. Eng. Sci. 9 (1959) 266.
[25] B.A. Bidingmeyer, F.V. Warren Jr., Anal. Chem. 56 (14) (1984) 1583A.